Available online at www.sciencedirect.com
SCIENCE DIRECT®
Continental Shelf Research 24 (2004) 149–165
CONTINENTAL SHELF RESEARCH
www.elsevier.com/locate/csr

Impact of a winter upwelling event on the distribution and transport of sardine (*Sardina pilchardus*) eggs and larvae off western Iberia: a retention mechanism

A.M.P. Santos[a,*], A. Peliz[a], J. Dubert[b], P.B. Oliveira[a], M.M. Angélico[a], P. Ré[c]

[a] *Instituto Nacional de Investigação Agrária e das Pescas (INIAP)-IPIMAR, Av. Brasília s/n, 1449-006 Lisboa, Portugal*
[b] *Departamento de Física, Universidade de Aveiro, Campus Universitário de Santiago, 3810-193 Aveiro, Portugal*
[c] *Laboratório Marítimo da Guia, Faculdade de Ciências da Universidade de Lisboa, Est. do Guincho, 2770 Cascais, Portugal*

Received 26 June 2002; received in revised form 26 September 2003; accepted 17 October 2003

Abstract

A hydrographic and ichthyoplanktonic survey was conducted on the western Iberia Peninsula shelf-slope, with the objective of assessing the influence of wind-driven flow on the transport and survival of sardine early life history stages. Measurements were taken during a 2-week period of an 'upwelling-favourable' wind event. An offshore displacement of the surface low salinity Western Iberia Buoyant Plume (WIBP) was observed well off the shelf break. Below the plume, the current was southward over the mid- and inner-shelf. Offshore, the flow was poleward in the northern part of the survey area and equatorward in the south. A convergence zone was detected along the outer shelf and upper slope where the buoyant plume was apparently trapped and deepened. In general, eggs and larvae were distributed according to the spreading of the low salinity surface waters, and also within the convergent band. Older larvae were retained within the latter feature. The role of wind forcing on the plume and its interaction with the slope flow were analysed. A mechanism of larvae retention was formulated based on simplified models of the observed shelf-slope circulation.

Keywords: Coastal upwelling; Ichthyoplankton; Oceanic convergences; Sardine; *Sardina pilchardus*; Transport processes; Western Iberian Peninsula; Portugal (40–42°N; 8–10°W)

1. Introduction

Over the last decades significant changes in the upwelling patterns off the Portuguese west coast have been observed (e.g., Santos et al., 2001; Borges et al., 2003), namely an increase in upwelling events in winter due to an increase in the frequency and intensity of equatorward winds observed since the end of the 1960s (Borges et al., 2003).

The maximum intensity of sardine (*Sardina pilchardus* Walbaum, 1792) spawning off Portugal takes place predominantly from November through April (Figueiredo and Santos, 1989; Ré et al., 1990; Zwolinski et al., 2001). The reproductive strategies of some pelagic fish adapted to coastal upwelling ecosystems, such as sardine on the Portuguese west coast, have developed to minimise Ekman offshore transport effects and assure shoreward transport and larval retention

*Corresponding author. Tel.: +351-21-302-7193; fax: +351-21-301-5948.
E-mail address: amsantos@ipimar.pt (A.M.P. Santos).

0278-4343/$ - see front matter
doi:10.1016/j.csr.2003.10.004

(e.g., Roy et al., 1989). Therefore, an increase in upwelling events during the spawning period may have a negative impact on sardine recruitment because of the increased larval mortality through offshore transport into unfavourable areas.

Santos et al. (2001) found statistically that the intensity and frequency of upwelling events during the spawning season (winter) does indeed have a negative impact on the recruitment of small pelagic species off the west coast of Portugal, limiting its success even if beneficial upwelling conditions occur later during the summer upwelling (feeding) season. Stratoudakis et al. (2003) also found a significant reduction in the sardine spawning area in north-western Portugal in the late 1990s.

To test the hypothesis that the occurrence of upwelling events during the spawning season (winter) can significantly affect the distribution of sardine early life stages and their survival, an observational programme was conducted off northern Portugal in February 2000.

The distribution and offshore transport of sardine eggs and larvae may not be determined only by wind action. Other local features constrain the surface response to coastal upwelling; namely the Western Iberia Buoyant Plume (WIBP) (Peliz et al., 2002), the Iberian Poleward Current (IPC) (Peliz et al., 2003b) and its associated mesoscale structures, as well as the interaction between the poleward flow and the buoyant plume.

The aim of this paper is to present the results of the observed distribution and abundance of sardine eggs and larvae in relation to the main ocean features of the upper layer and shelf waters during an upwelling event. To simulate the major patterns of eggs and larval transport a derived two-dimensional flow field was calculated, based on simplified estimates of the circulation features during the survey, and a set of Lagrangian particles are tracked in the sampled area. Finally, a conceptual model of the retention mechanism is presented and discussed.

2. Study area, data and methods

The SURVIVAL'2000 cruise (02040200) took place off the northwest Portuguese coast onboard IPIMAR's R/V *NORUEGA*. Five transects were made perpendicular to the coast between Viana do Castelo (41.6°N) and Figueira da Foz (40.4°N) from February 16 to 20, 2000 (Fig. 1). Two current meter mooring arrays were deployed at the beginning of the survey.

Hydrographic parameters were measured at all the stations using a SBE 9p CTD in its first use after factory calibration with a sampling rate adjusted to 12 or 24 scans every second and a lowering rate of about 1 m/s. Chlorophyll concentrations were measured with a Seapoint fluorometer coupled to the CTD. Water samples for calibration were collected in all stations with a carousel sampler. Water salinity was measured in the laboratory using a Guideline Autosal 8400B Salinometer. A total of 365 salinity samples were

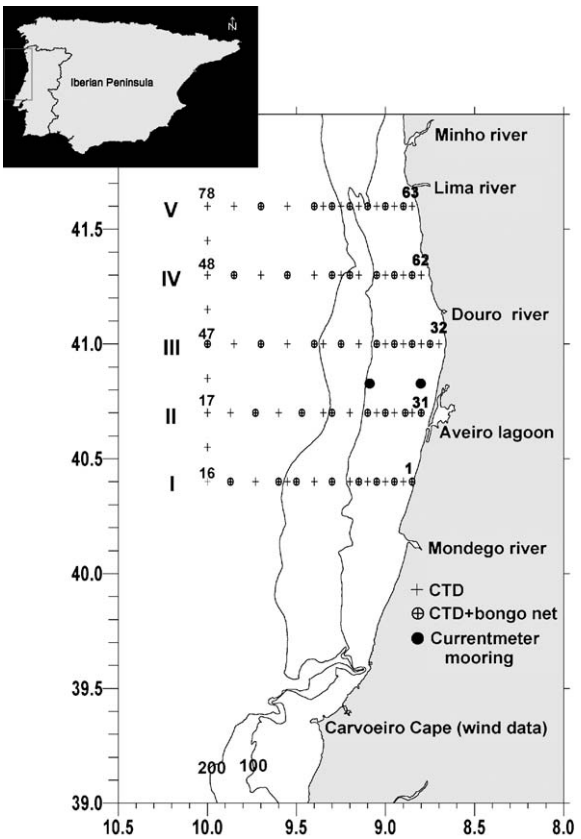

Fig. 1. Study area (northwestern Portuguese coast), cruise sampling grid and current meter mooring location. The 100 and 200 m bathymetry lines are shown.

used to calibrate the conductivity data. Standard algorithms (Fofonoff and Millard, 1983) were used to compute salinity and density. Flourometer data were calibrated according to the methodology described in Ribeiro et al. (submitted for publication).

Current meter data were obtained with three Aanderaa RCM 9 instruments in two mooring arrays: one deployed over the 80 m isobath with two current meters at depths of about 20 and 50 m, respectively; and the second over the 30 m isobath with one current meter at about 20 m depth. The data were low-pass filtered to remove tidal and inertial oscillations and the final time series represent the residual currents.

Fish eggs and larvae were sampled using a bongo net of 60 cm mouth diameter fitted with 500 and 335 μm mesh nets. A single Hydro-Bios flowmeter was fitted on the side of the 335 μm mesh net to compute the volume of water filtered during each haul. All hauls were taken at a speed of 2 knots. Sampling was carried out to a maximum depth of 50 m, or about 5 m above the bottom where the water depth was shallower. A total of 97 oblique hauls were obtained at selected stations (Fig. 1). Plankton samples (335 μm) were fixed immediately after collection with 4% buffered formalin. In the laboratory, fish eggs and larvae were sorted and counted. Larval lengths were measured with the aid of a binocular microscope to the nearest 0.5 mm by placing the larva on a transparent grid marked in millimeters and illuminated from below. All larval lengths correspond to standard lengths corrected for shrinkage (live length) according to Theilacker (1980).

3. The wind event and circulation at the slope

The wind during 15 January to 15 March 2000 at the meteorological station of Cape Carvoeiro (Portuguese Meteorological Office) is presented in Fig. 2. This station is located several tens of kilometres to the south of the sampled area but no important differences over this distance are expected in the wind fields. The most significant southward upwelling event started a few days before the cruise and had a duration of about 2 weeks, including a slight relaxation around 20 February. Although persistent in direction, the wind intensity was not very strong, with maximum velocities of about 5–8 m/s. Before the cruise the wind varied mainly between episodes of southerly and southeasterly winds, but with lighter intensity.

Fig. 3 is an attempt to collect together the most important features capable of influencing the surface circulation and the transport patterns. The horizontal distribution of temperature at 100 m, the shallowest level out of the influence of the surface buoyant plume (Fig. 3a), and the corresponding geostrophic velocity field at 100 m calculated relative to the 1350 dbar level (under the Mediterranean water main core) show the three

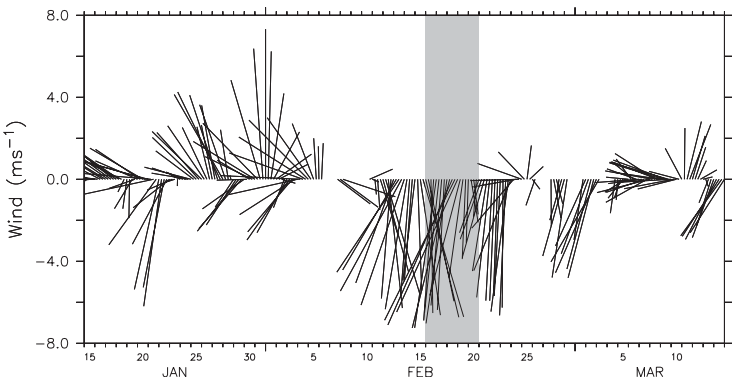

Fig. 2. Stick diagram of wind (m/s) measured at Cabo Carvoeiro (9.40°W; 39.36°N) by the Portuguese Meteorological Office between 15 January and 15 March 2002 (negative values correspond to north winds).

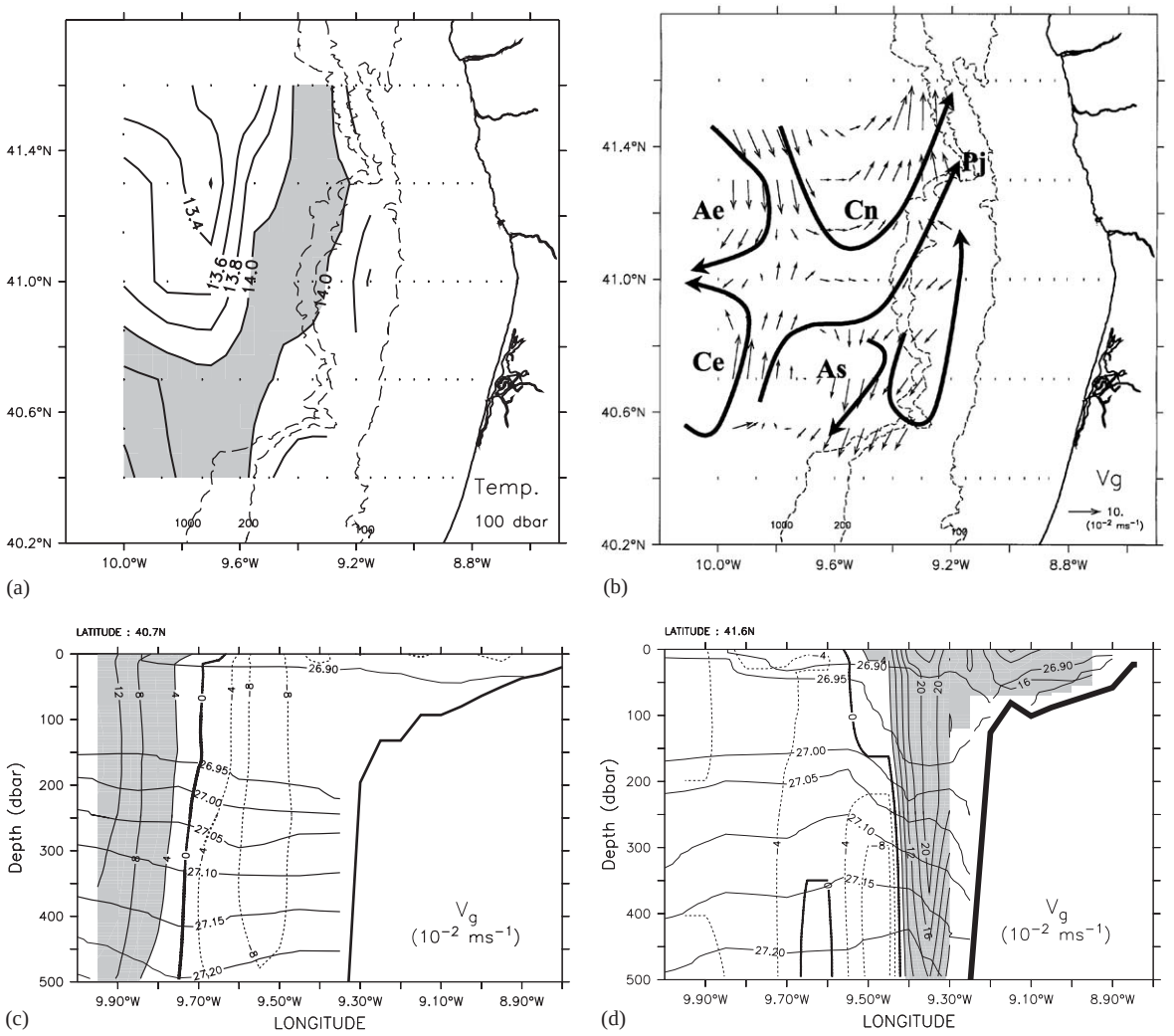

Fig. 3. Horizontal distributions of (a) temperature at 100 dbar (°C; values >14°C are in shaded) and (b) geostrophic velocity (cm/s) referred to 1350 dbar at 100 m depth, and vertical fields of geostrophic velocity (cm/s) referred to 1350 dbar superimposed in density fields (σ_t) for (c) section II (40.7°N) and (d) section V (41.6°N). Poleward flow is shaded in vertical fields. Cn and Ce represent cyclonic eddies, Ae and As represent anticyclonic eddies, and Pj is the poleward slope jet (see text for details).

most prominent circulation features (Fig. 3b). The first is an anticyclone in the south (As—centred at about 9.8°W and 40.7°N) coincident with a zone of warm waters. This feature induces southward flow over the slope in the southern half of the sampled area as seen in the geostrophic velocities in section II (Fig. 3c). At the same time, a cyclonic meander (Cn—centred at about 9.6°W, 41.4°N) associated with a cold intrusion (Fig. 3a,b) and a poleward slope jet (Pj) with velocities up to 0.25 m/s, transporting warmer and saltier waters northward, dominated the northern part of the survey (Fig. 3d). An additional cyclone–anticyclone pair seaward of the first structures was also detected. Here, the cyclone was in the south (Ce) and the anticyclone in the north (Ae).

These circulation structures are not strongly influenced by the wind event, but have a significant influence on the response of the surface layer as discussed below. The most relevant contribution is

the meridional advection of the plume waters that are transported off the shelf by the Ekman dynamics. In the northern part, the poleward slope jet is strong enough to constrain Ekman transport, as will be seen later, in contrast to the southern area, where the flow is broader and slower.

4. Response of the upper layer and buoyant plume dynamics

The WIBP is a low salinity surface water fed by the winter-intensified runoff of several rivers on the northwest coast of Portugal and Spain (Fig. 1, Minho, Mondego, Douro, Lima, Vouga). During typical non-upwelling winter conditions, the plume is confined to the inner-shelf from the Mondego river mouth northward with salinity values less than 35.7–35.8 psu (Peliz et al., 2002). Salinity minima are variable and are usually located in patches close to the estuaries. Because of their higher buoyancy, the surface waters in the plume also exchange heat with the atmosphere in a different way from the surrounding waters as the thermally driven convection is limited to a thinner layer. This contributes to a faster cooling of plume waters, which are usually cooler at their estuarine source. This leads to the plume waters having lower temperatures than surrounding offshore waters and they may even be colder than the waters beneath. This thermal contrast between plume and oceanic waters is enhanced when the IPC is intensified, as this current transports warmer and saltier waters poleward along the slope.

The most remarkable observation in the surface hydrographic fields is the unusual offshore extension of the WIBP (Fig. 4), as a first consequence of the seaward transport of low salinity surface waters (minimum <35.2) inside the surface Ekman layer. However, the plume is not transported offshore as a continuous feature, as its separation from the coast is detected only in a narrow band less than 20 km wide as verified by the presence of salinity values above 35.7 near the shore (e.g., Fig. 4b). Its offshore extension is about 100 km, in the centre of the sampling area, and it is separated into two main patches located just offshore of the shelf break, one at 9.4°W, 40.7°N and the other at 9.2°W, 41.6°N. This means that factors other than offshore advection are involved in the response of the plume to the upwelling-favourable winds.

The observed patches may have originated at the coast as pools of direct river output in the vicinity of the river mouths; however, their evolution most likely resulted from the interaction of the stratified Ekman layer with the circulation at the slope. The Ekman dynamics cause an offshore displacement of the plume crossing the upper slope current ageostrophically and, in turn, the poleward flow forces a northward advection. Moreover, the several mesoscale features associated with the poleward current will condition the further advection and mixing of the plume.

The zone where the plume is disrupted (9.6°W, 41.2°N; Fig. 4b) coincides with the cyclonic meander, whereas the larger patch of the plume in the south coincides with the anticyclone observed over the slope (Fig. 3b). The plume is generally evident northward and coastward along the flow of the IPC.

Once beyond the slope, the plume interacts with the offshore cyclone and anticyclone. These create a confluence zone between them that is coincident with the westernmost limit of the plume (at about 9.8°W, 41.0°N). Ribeiro et al. (submitted for publication) in a sequential analysis of satellite-derived pigment concentrations, detected the offshore advection of the high-pigment-concentration plume, which is schematically represented in Fig. 5. The plume expands offshore and its maximum offshore extension is coincident with a filament located in the confluence zone described above with maximum velocities of 29.3 km/day (Ribeiro et al., submitted for publication). Elsewhere, the seaward advection of the front was obstructed by the along-slope flow.

In general, the plume is thicker on its coastward side (note the salinity and density distributions in the various sections of Figs. 6 and 7). This type of structure is generated in the process of plume advection forced by Ekman layer dynamics. Fong and Geyer (2001) modelled the response of a buoyant plume to upwelling-favourable wind and found an asymmetry between the front and the

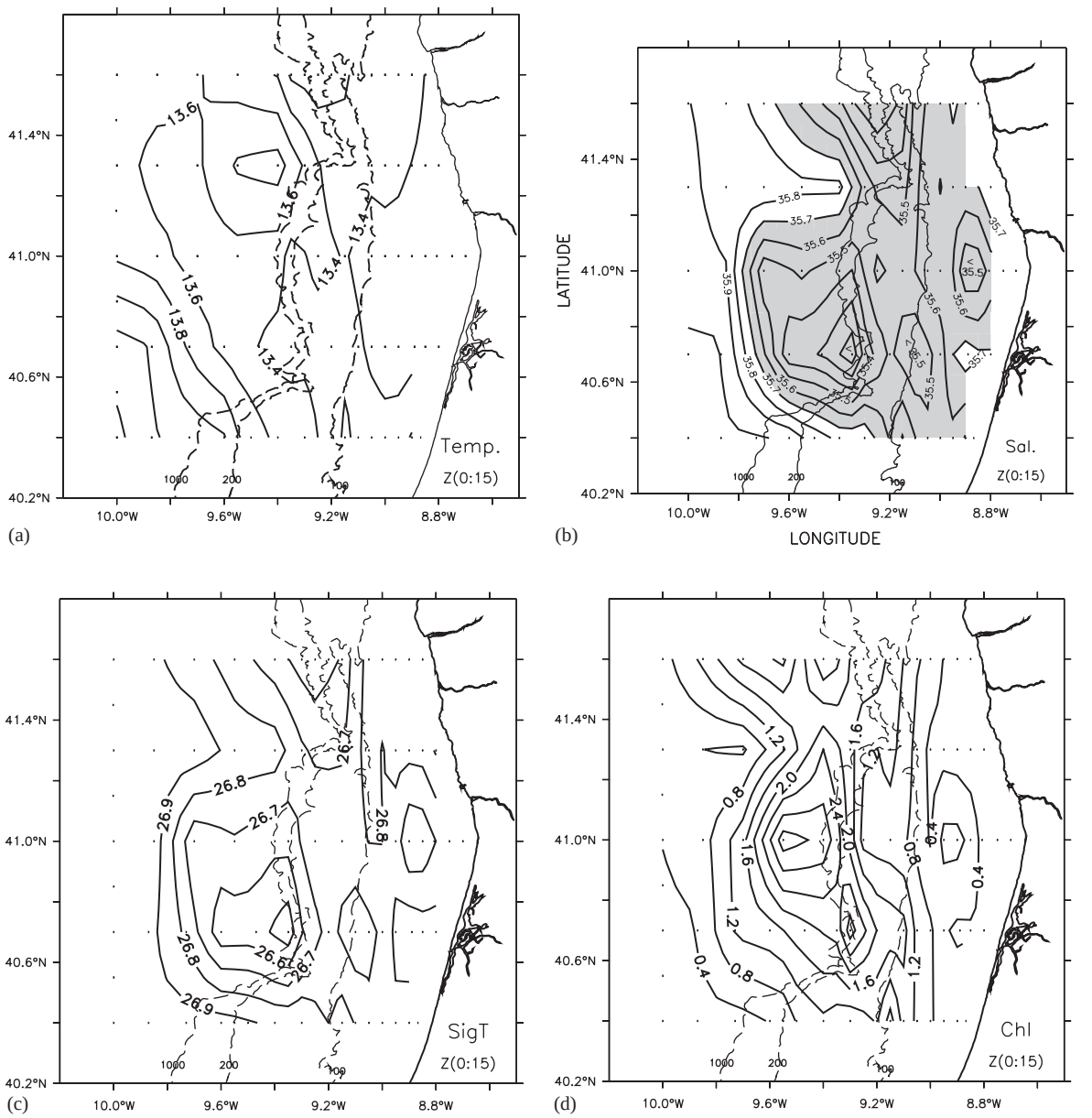

Fig. 4. Horizontal distributions (0–15 m) of (a) temperature (°C), (b) salinity, (c) density (σ_t), and (d) chlorophyll-*a* concentration (mg/m^3). The WIBP is shaded in (b).

rear side of the plume. The seaward side tends to become more stratified once lighter plume waters are advected above the denser offshore waters. This increase in the stratification makes the Ekman layer thinner (e.g., Lentz, 1992; Price and Sundermayer, 1999). The inner side of the plume has a different evolution. Ekman transport brings denser waters into the plume, which then overturns, deepens and gains volume by mixing with deeper waters. This process is repeated until the coastward side of the plume becomes significantly mixed as in the example of section IV (Fig. 7b).

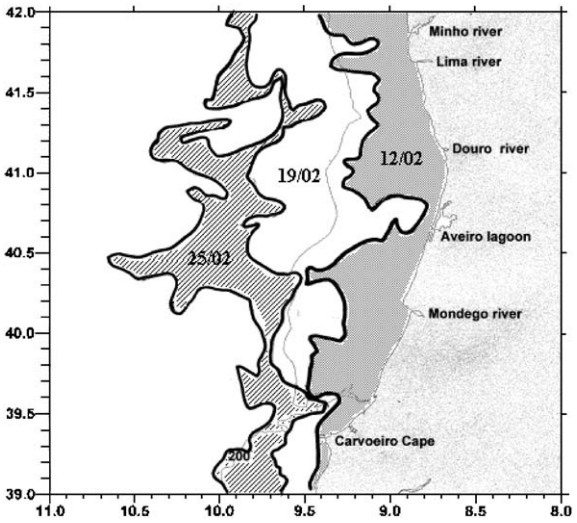

Fig. 5. Spatial and temporal progression of the chlorophyll-*a* front derived from ocean colour satellite data (SeaWiFS sensor onboard Orb View-2 satellite), on 12, 19 and 25 February 2000. The thin line represents the 200 m isobath (adapted from Ribeiro et al., submitted for publication).

Another important component of the upper layer response to the upwelling event concerns the phytopigment concentration growth (Fig. 6d). The Ekman layer was nearly coincident with the stratified upper layer and almost all the surface transport consisted of a westward advection and horizontal spreading of the plume, with little entrainment of the offshore deep mixed layer. This provided a vertical retention mechanism that constrained the biological response of the system in an unexpected way, in view of the typical winter response of deep (100–150 m) low-nutrient mixed layers. Thus, the offshore concentration of phytoplankton is relatively high. Ribeiro et al. (submitted for publication) registered a significant growth proportional to the enlargement of the plume area. This phytoplankton development was supported by the stratification maintained in the process of offshore advection of the plume, as becomes obvious in the comparison between the surface phytopigment concentrations (Fig. 4d) and the stratification inside the plume (Fig. 8). A more detailed discussion about the process of phytoplankton biomass response to the upwelling event can be found in Ribeiro et al. (submitted for publication).

5. The inner shelf and the convergence zone

Over the inner shelf, southward flow directly measured by the three current meters placed on the two moorings show that the upwelling event had two main bursts with a short relaxation in between (Fig. 9). The intensities indicate that the event was significant, although no strong upwelling jets were generated (maximum sub-inertial values are about 0.15 m/s southward in the inner mooring—not shown). However, despite the evidence of upwelling, the surface plume waters were not completely advected off the shelf. Indeed, as some were transported offshore, others were advected southward along the shelf. This picture contrasts with the one described before, for the outer shelf, where a northward flow was observed in the northern part of the slope. This change of flow direction observed at the outer shelf is associated with a convergence band oriented along-coast that extends throughout all the sampled area.

In the vertical distributions (Figs. 6 and 7), the interaction between the plume and the IPC is evident. As the plume expands offshore, it will interact with the poleward flow creating conditions for a convergence at the surface. The mechanism for convergence results from the fact that the along slope flow acts as a barrier to the surface Ekman transport. The poleward flow is intense and perpendicular to the Ekman transport and it is expected that part of the plume be retained there. However, if the wind-driven surface transport is significantly intense and persistent, the shelf waters can cross over the poleward current. Fig. 6a is a good example of this interaction: the plume waters are cooler than the poleward flow, which can be identified by the closed 14°C temperature contour.

Another factor likely to contribute to the retention of the plume is the vertical circulation associated with the upwelling dynamics. In the case of a deep mixed layer and moderate alongshore currents, replacement of the surface waters is done from the interior layer (e.g., Allen et al.,

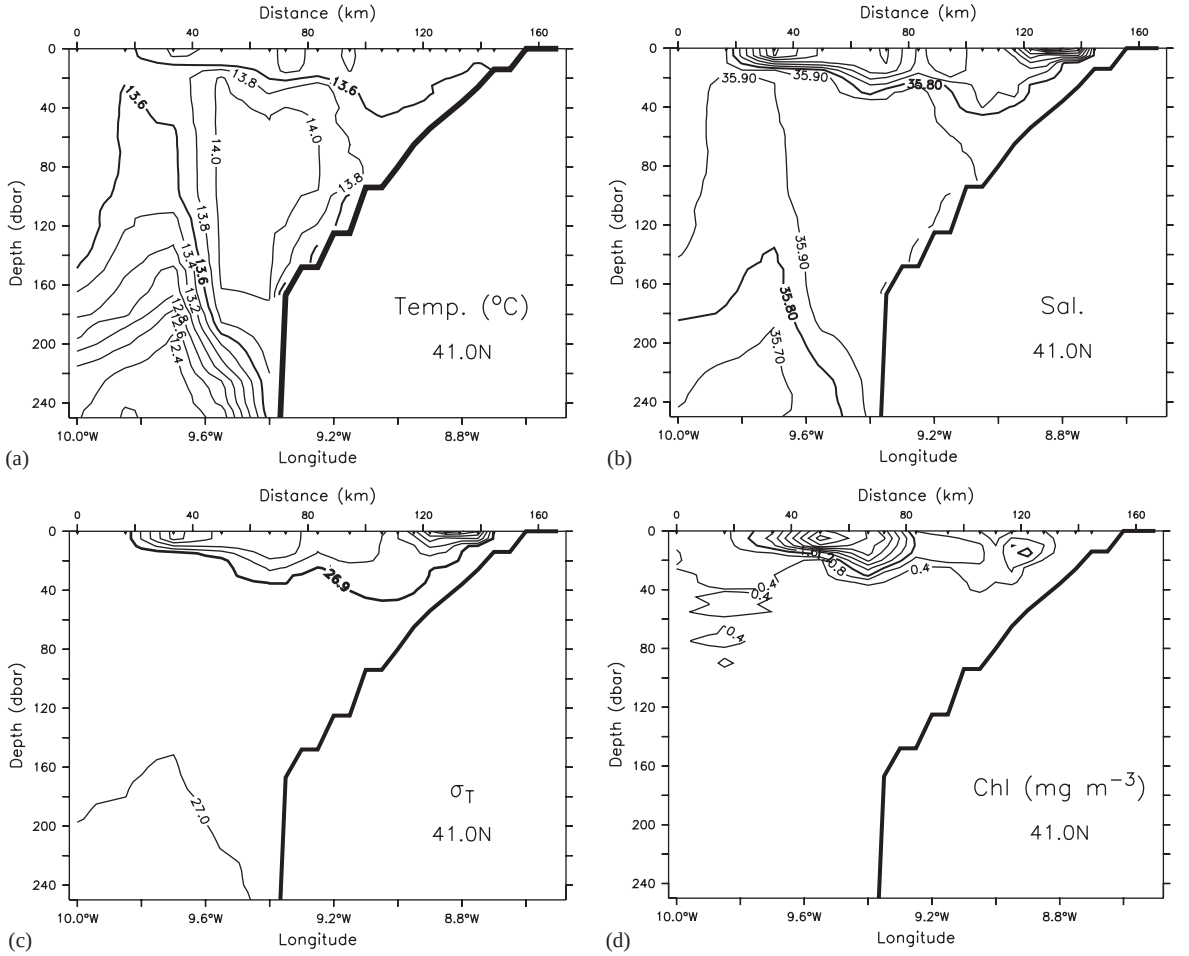

Fig. 6. Vertical fields of section III (41.0°N): (a) temperature (°C), (b) salinity, (c) density (σ_t), and (d) chlorophyll-*a* concentration (mg/m^3).

1995), and the vertical circulation is closed at the outer shelf through a surface convergence of the upwelled waters. A deepening of the plume close to the outer shelf was observed throughout the sampled area and is coincident with the change in the slope of the isopycnals. This pattern can be seen in the topography of the 35.8 isohaline surface (considered to be an indication of the deepest limit of the plume) in Fig. 10. In the northern half of the sampled area this shelf zone also coincides with a change in the direction of the along-shore flow: northward at the upper slope and southward from the mid-shelf up to the coast.

The plume deepens in the outer shelf more remarkably in the northern part where the poleward slope flow is increased (see the maximum of 55 m at about 9.1°W, 41.3°N in Fig. 10). This indicates that bottom Ekman layer dynamics, as described in Peliz et al. (2003a), may contribute to the generation of this convergence band. These authors conducted a numerical study of the response of the shelf/slope system with an along-slope current to upwelling-favourable winds, similar to the situation described here. They found that a divergence in the bottom Ekman layer occurs due to the change in orientation of the

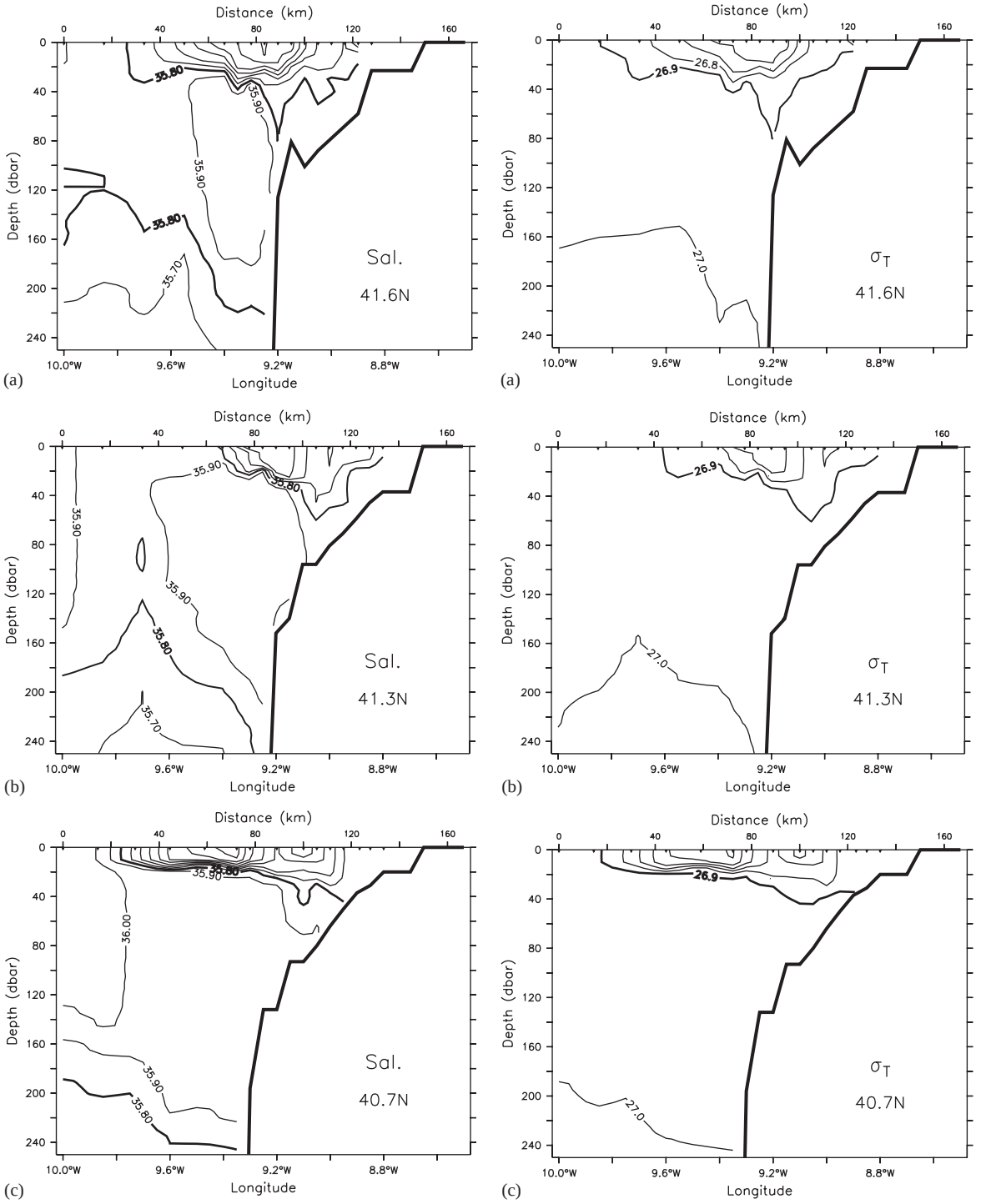

Fig. 7. Vertical fields of salinity (left) and density (σ_t; right) for: (a) section V (41.6°N), (b) section IV (41.3°N), and (c) section II (40.7°N).

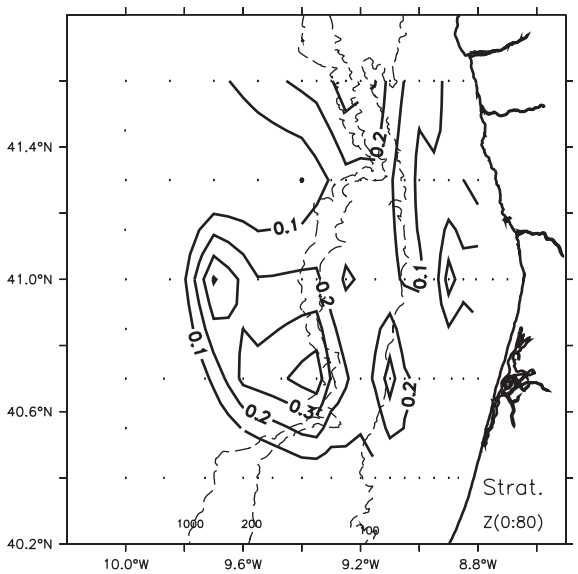

Fig. 8. Stratification of the 35.8 isohaline calculated as the density difference between the 5 m depth and the depth of the buoyant plume determined by the 35.8 isohaline surface.

along-slope flow. Along the slope and outer shelf the flow is northward and the transport inside the bottom Ekman layer is downslope. At the same time, over the shelf the flow is southward and the bottom layer transports water coastward. This divergence at the outer shelf is compensated by a downward mass flux with deepening of the isopycnals and the low salinity plume at that point (Fig. 7). The stratification in the temperature and salinity of the bottom layer over the outer shelf in sections III and V (Figs. 6a, b and 7a) may also be caused by the downslope transport associated with the poleward flow. This process could be responsible for the thickening of the plume, and also for it being trapped in that part of the shelf, thus constituting another constraint for offshore transport of the low salinity waters of the plume and all the biological material within it.

6. Ichthyoplankton distribution

The distribution of sardine eggs and larvae, as well as of all other fish eggs, is shown in Fig. 11. Fish eggs were found mainly in the outer shelf with the highest concentrations over the shelf break (Fig. 11a). There is a clear association between the offshore distribution of the eggs and the area of influence of the buoyant plume (Figs. 4b and 8). The stations with most eggs over the shelf are also located in zones where the influence of the plume is more significant. As far as sardine eggs are concerned (Fig. 11b), they were mainly distributed over the shelf break, especially in the north, and only a small number were detected in the inner part of the shelf in the south. This indicates either an increased vulnerability of the sardine eggs to Ekman transport or that the spawning occurred at the outer shelf. However, sardine spawning is considered to be restricted to the continental shelf as observed from ichthyoplancton surveys (Ré et al., 1990) and from the distribution of adult fish (e.g., Dias et al., 1989; ICES, 2001). The adult distribution area rarely extends beyond the 100 m isobath. The occurrence of sardine eggs in the inner shelf in the south of the surveyed area (Fig. 11b) also suggests that spawning was mainly occurring over the continental shelf.

Fig. 11c shows the distribution of sardine larvae. There is not any significant difference in relation to the distribution of the eggs. However, it is clear that a considerable number of larvae were sampled at the shelf break in the southern part of the surveyed area.

However, the most interesting pattern is the spatial distribution of the mean length of the larvae presented in Fig. 11d, in which two patterns are identified: a meridional gradient in the mean length of larvae with the smaller ones mainly in the southern stations and the larger ones in the northern stations; and a cross-shore gradient with larger larvae found further offshore. Thus the observed distributions seem to indicate an offshore advection, especially in the southern part where the WIBP is observed to be spread further offshore (Fig. 4b), and also northward transport of the sardine larvae, with retention at the convergence zone. Note that the higher mean length of sardine larvae associated with northern stations is statistically significant as tested by one-way ANOVA (Table 1), as well as the inshore/offshore differences (Table 2).

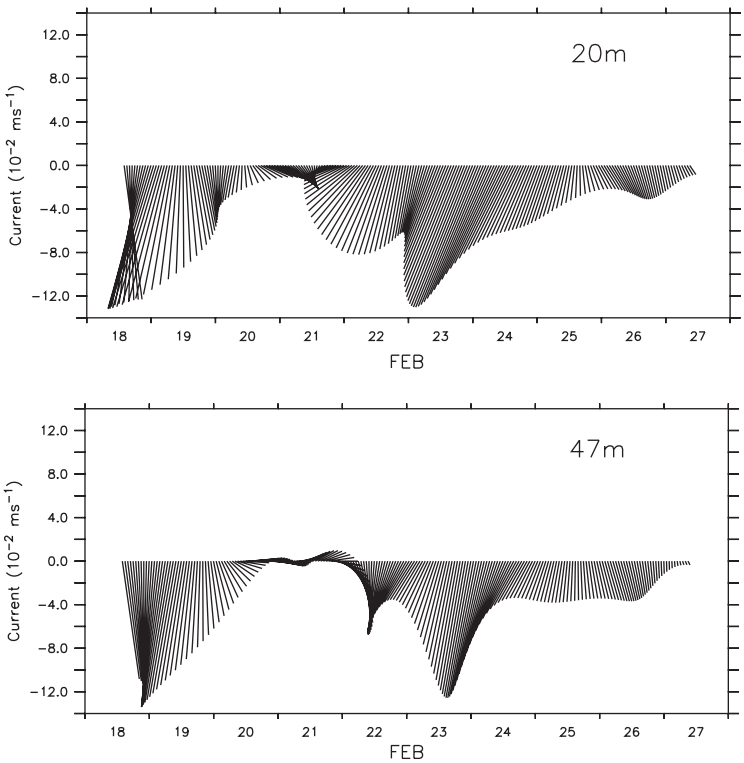

Fig. 9. Stick diagram of current meter measurements (cm/s; one stick every hour) at the mooring array located at the 80 m isobath (see Fig. 1 for location) from 18 to 27 February 2000: (a) current meter located at the 20 m depth level, and (b) current meter located at the 47 m depth level. Negative values correspond to equatorward currents.

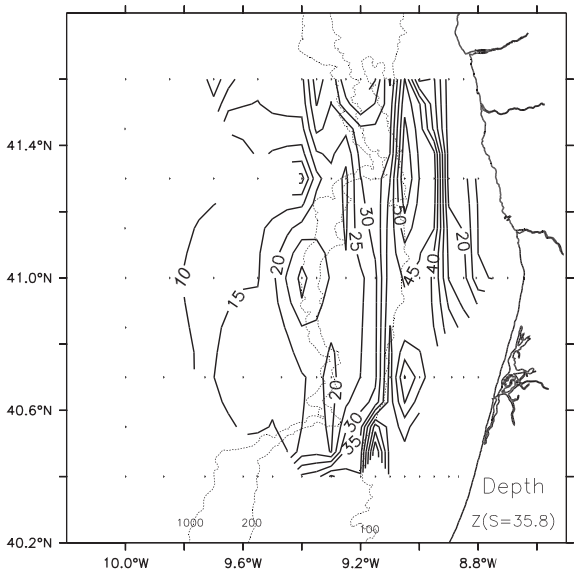

Fig. 10. Depth (m) of the 35.8 isohaline surface, which was considered representative of the lower boundary of the buoyant plume (WIBP).

7. A simple transport model

A time evolving surface flow field corresponding to the upwelling event from 18–22 February 2000 was estimated based on the information of the current meter data (Fig. 9), the calculated geostrophic currents (Fig. 3) and the wind-stress data (Fig. 2). The total surface velocity was calculated adding an Ekman layer velocity to the surface geostrophic flows beyond the 100 m depth zone and to the current meter derived velocities at the 100 m contour. The offshore velocity was estimated according to the expression:

$$\mathbf{v}_{\text{offshore}}(x, y, t) = \mathbf{v}_{\text{g}}(x, y) + \mathbf{v}_{\text{ek}}(t), \tag{1}$$

where $\mathbf{v}_{\text{g}}$ stands for the calculated geostrophical velocities and $\mathbf{v}_{\text{ek}}$ represents a time-evolving Ekman layer velocity.

Over the shelf the velocity was obtained by extrapolating the current meter time series at 47 m

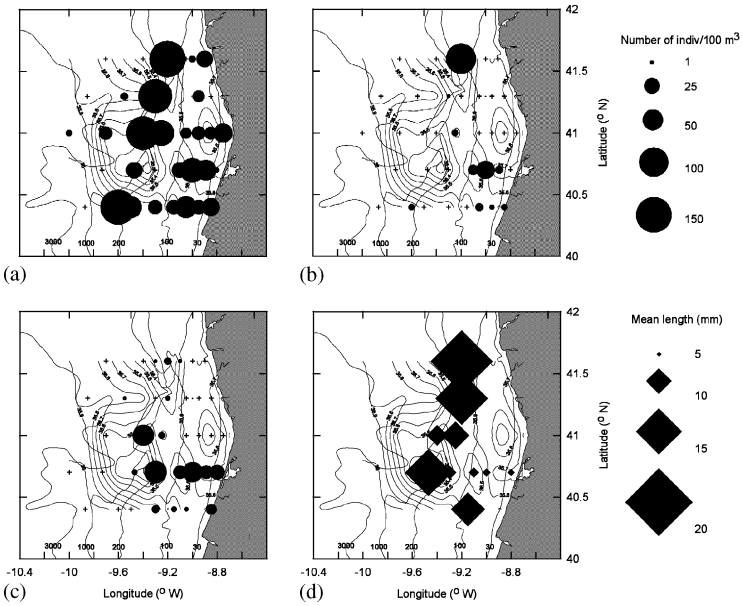

Fig. 11. Distribution and abundance of ichthyoplankton (0–50 m) superimposed on horizontal distribution (0–15 m) of salinity during February 2000: (a) number of fish eggs per 100 m^3; (b) number of sardine (*Sardina pilchardus*) eggs per 100 m^3; (c) number of sardine larvae per 100 m^3; and (d) mean length (mm) of sardine larvae. The thin lines represents the 30, 100, 200, 1000 and 3000 m bathymetry lines.

Table 1
Analysis of variance to test differences in the mean length of sardine larvae between northern (48–78) and southern (1–47) stations

Groups	Count	Sum	Average	Variance	
Southern stations	124	899.63	7.26	5.32	
Northern stations	18	316.63	17.59	12.29	
Source of variation	*SS*	*df*	*MS*	*F*	*P*-value
ANOVA					
Between groups	1679.06	1	1679.06	272.24	<0.001
Within groups	863.47	140	6.17		
Total	2542.53	141			

depth, which was considered representative of the interior velocity at the shelf, ($\mathbf{v}_c(t)$) throughout the shelf zone (although the differences are small in Fig. 9, the upper current meter (at 20 m) still shows some possible local influence of the plume):

$$\mathbf{v}_{\text{inshore}}(x, y, t) = \mathbf{v}_c(t) + \mathbf{v}_{ek}(t). \quad (2)$$

The choice of Eq. (1) or Eq. (2) was based on the local depth. The velocities in grid points shallower than 100 m were calculated with Eq. (2), and all the remaining velocity estimates were obtained with Eq. (1). The Ekman velocities were calculated using the expression $v_{ek} = \tau/(\rho df)$ (e.g., Cushman-Roisin, 1994), where ρ is the mean density, f the